Journal of Geochemical Exploration 200 (2019) 27–36

Contents lists available at ScienceDirect

Journal of Geochemical Exploration

journal homepage: www.elsevier.com/locate/gexplo

A review of Ni and Co incorporation during talc synthesis: Applications to crystal chemistry, industrial compounds and natural Ni- and Co-rich ore

François Martin[a,*], Cyril Aymonier[b], Sandra Einloft[c], Christel Carême[d], Mathilde Poirier[a], Marie Claverie[a,b,d], Manoela Argenton Prado[a,c], Guilherme Dias[a,c], Cyril Quilfen[b], Guillaume Aubert[b], Pierre Micoud[a], Christophe Le Roux[a], Stefano Salvi[a], Angela Dumas[a], Suzanne Féry-Forgues[e]

[a] GET UMR 5563 CNRS-UPS, Université de Toulouse III, OMP, ERT Géomatériaux, 14 Avenue Édouard Belin, 31400 Toulouse, France
[b] ICMCB UMR 5026 CNRS, Université de Bordeaux, 33600 Pessac, France
[c] Faculdade de Química (FAQUI), Pontifícia Universidade Católica do Rio Grande do Sul (PUCRS), Porto Alegre, Brazil
[d] IMERYS, 2 Place Édouard Bouillères, 31100 Toulouse, France
[e] SPCMIB UMR 5068 CNRS-UPS, Université Toulouse III, 118, route de Narbonne –Bât 2R1, 31062 Toulouse Cedex 09, France

ARTICLE INFO

Keywords:
Ni
Synthesis
Talc
Materials
Crystal growth

ABSTRACT

This article reviews the current knowledge on the incorporation of Ni and Co cations in mineral synthesis. In addition, it overviews the interest in developing such materials, and discusses a number applications in which these materials are used as mineral fillers. A reflection is then conducted showing that synthetic minerals rich in Ni and Co compare closely to those occurring in Ni- and Co-rich natural lateritic environment, which can thus be considered as mutual proxies. It follows that studies of lateritic environments can provide valuable information on formation processes of synthetic minerals, and vice versa. An example of cross-checking data between these two thematic fields is presented, which allows solving chemical fractionation problems encountered in lateritic environments.

1. Introduction

Clays constitute an abundant and cheap resource worldwide. Clays can find applications in many different fields, as they can induce new properties in ceramic, polymer, paper, cosmetic, pharmaceutical, oil drilling and isolation industries, and are also commonly used as mineral fillers in order to reduce production costs (Kloprogge et al., 1999). Among the T-O-T phyllosilicates, talc is the least complex, with the formula $Mg_3Si_4O_{10}(OH)_2$. This mineral has been known since the Antiquity for its softness and its whiteness when reduced to powder. Nowadays, the genesis of talc deposits is well understood, and it is recognized that the broad spectrum of conditions that can lead to its formation can explain the wide diversity in color, grain size, crystallinity, lamellar-character, softness, chemical composition and presence of accessory minerals such as chlorite and carbonates, found in different deposits (Zazenski et al., 1995; Robert and Fragnier, 1996; Soriano et al., 1998, 2002). However, as usages of talc in industry evolve towards more and more complex applications, new requirements and limitations emerge, such as (i) the need for extreme talc ore purity, particularly in cosmetic and pharmacologic uses; (ii) problems related to the difficulty in dispersing talc in water, and (iii) the need to use submicrometric talc particles to develop polymer-based nanocomposites (Usuki et al., 1993a, 1993b; Kojima et al., 1993a, 1993b). To satisfy these requirements, a number of measures were taken by different workers: (i) the need of high-purity talc was solved by searching for new, highly pure talc deposit (Misch et al., 2018) and by improving talc ore purifying techniques (Baba et al., 2015; Castillo et al., 2014; Dumas et al., 2015a); (ii) improvement of the ability to disperse talc dispersion in water was achieved by surface treatments such as pre-coating by carboxyl-methyl cellulose adsorption (e.g., Bonino et al., 2002; Bacchin et al., 2006); and (iii) the need of submicrometric talc particles led to the development of new grinding processes such as air-jet milling, sonication, stirred-ball milling and dry milling (Godet, 2001). Nevertheless, using these so-called top-down approaches was not as satisfactory as hoped, because to grind natural talc to below 1 μm in size, homogeneously, invariably led to amorphization and disordering of its

* Corresponding author.
E-mail addresses: francois.martin@get.omp.eu (F. Martin), cyril.aymonier@icmcb.cnrs.fr (C. Aymonier), Einloft@pucrs.brc (S. Einloft), Christel.Careme@imerys.com (C. Carême), sff@chimie.ups-tlse.fr (S. Féry-Forgues).

https://doi.org/10.1016/j.gexplo.2019.02.002
Received 26 March 2018; Received in revised form 17 January 2019; Accepted 9 February 2019
Available online 11 February 2019
0375-6742/

structure (Liao and Senna, 1992; Sanchez-Soto et al., 1997; Dellisanti et al., 2009; Cavajda et al., 2015; Borges et al., 2016). It is within this context that most research in the last couple of decades has focused on bottom-up approaches, including the technique of hydrothermal synthesis, in the hope of obtaining a combination of the three sought parameters (purity, nano-size without amorphization of the structure and hydrophilic character) (Martin et al., 1992, 1996; Martin, 1994; Dumas et al., 2011a; Martin et al., 2006; Lèbre, 2007; Arseguel et al., 2006; Le Roux et al., 2010; Dumas et al., 2013a, 2013b; Dumas, 2013; Claverie et al., 2018). In collaboration with industrial partners (IMERYS), synthesis processes were recently revised and optimized, resulting in a simpler, faster, and more efficient process that complies with industrial requirements. Preparation of synthetic talc requires two steps: (i) preparation of a talc precursor at room temperature with the appropriate Mg/Si ratio and (ii) a hydrothermal treatment. Currently, synthetic talc is used in various industrial sectors as a competitive and innovative filler, and it is forecasted that the demand for this novel material will lead to a significant technological transfer within the year.

However, before scaling up the process, crystallogenetic mechanisms should be considered. Although synthetic talc is a well-documented product, very little information is available on the precursor material. Some authors confirmed its amorphous character and revealed a highly agglomerated and porous (micropores and mesopores) product (Dietemann, 2012; Dietemann et al., 2013; Claverie et al., 2018). Moreover, understanding the growth mechanisms of synthetic talc can help shedding light on the crystallization of talc in a variety of natural settings, including low- (sedimentary, weathering) as well as high-temperature (metamorphic, hydrothermal) geological environments.

Typical techniques used to investigate natural talc growth mechanism include diffraction and spectroscopic methods, while X-ray diffraction (XRD) data is generally used to gain information on its crystalline structure at the scale of approximately 50 Å. Techniques such as Fourier transform infrared spectroscopy (FTIR) and X-ray absorption spectroscopy (XAS) can provides details on the local structure. Extended X-ray absorption fine structure (EXAFS) is an excellent technique to probe the immediate environment of the octahedral cations, as it can provide the distances and coordination number (CN) of the octahedral absorbing atoms. The procedure of talc synthesis allows partial to complete substitution of the magnesium cation in the octahedral sheet by a nickel cation (ionic radius of 0.69 and 0.72 Å for Ni and Mg, respectively). The fact that the energy absorption of Ni atoms is more easily measured by EXAFS than that of Mg atoms (8333 and 1305 eV for Ni and Mg, respectively) resulted in an increased production of studies on synthetic Ni-talcs (Dumas et al., 2015b).

This note aims to review the potential of talc nanoparticles, particularly, Ni-bearing talc particles. We focus on the processes used to produce synthetic talc in a very short time, on the transition from prototalc (i.e., talc precursor) to talc using variable Ni and Mg ratios in the octahedral layer, and on the prospect to use synthetic Ni-talc to evaluate dispersion into polymer matrixes by monitoring its green color. Similar observations may be done using Co cations, as they can easily replace Ni and Mg in the TOT structure during hydrothermal synthesis. In natural lateritic environments, it is Mn oxides that are commonly regarded as the major Co-bearing minerals (Dublet et al., 2017), while TOT phases are generally not considered.

2. The talc synthesis process

Talc is a hydroxylated magnesium phyllosilicate (sheet silicate), with the formula $Mg_3Si_4O_{10}(OH)_2$. It is the simplest pole of 2:1 type phyllosilicates. It is constituted by a stack of a large number of sheets along the c* axis (Fig. 1). Each sheet is composed of a hydrophilic octahedral $MgO_4(OH)_2$ layer, covalently bonded to two hydrophobic SiO_4 tetrahedral layers. Because the 2:1 (or TOT) sheets of talc are electrically neutral, no ion or water molecule is present in the interfoliar space. The sheets are connected to each other by Van der Waals electrostatic forces, which explains the relative ease in slipping talc sheets relative to each other when the grain is subjected to tangential shearing.

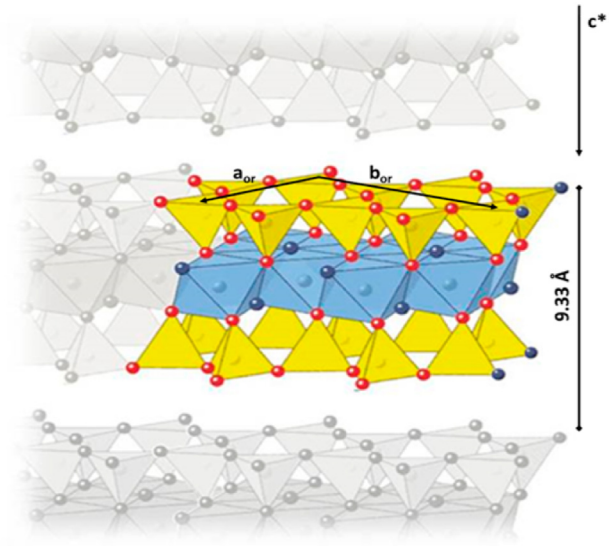

Fig. 1. Structure of talc (2:1 phyllosilicate); yellow ball: silicon; light blue ball: magnesium; dark blue ball: hydroxide; red ball: oxygen. (For interpretation of the references to color in this figure legend, the reader is referred to the web version of this article.)

The review paper by Claverie et al. (2018) summarizes the history of talc synthesis since its beginning, during the 1950s. In brief, the first synthesis trial was carried out at high temperatures (> 700 °C). Subsequently, at least until 2014, workers used hydrothermal of "batch" type or closed reactors, generally between 200 and 500 °C (Fig. 2). The quantities of products obtained were of a few tens of grams, which was enough for crystallochemical and crystallographic studies (Chabrol et al., 2010; Dumas et al., 2013a, 2013b; Dumas, 2013; Martin, 1994; Martin et al., 1992, 1996; Lèbre, 2007).

To screen the potential of synthetic talcs in some applications, IMERYS decided to finance a large batch reactor to obtain around 1 kg of product at the end of one run (Fig. 3). Encouraged by the good results, in 2015 IMERYS continued funding studies to test alternative ways of manufacturing talc, with the objective of producing it in a continuous mode. It turned out that under supercritical conditions, synthesis times could be reduced to only a few tens of seconds, a major achievement compared to the nearly 10 h required to run a complete production cycle in a closed reactor (Aymonier et al., 2014). Based on the techniques developed by Aymonier's group at the ICMCB lab in Bordeaux (Reveron et al., 2006; Aymonier et al., 2007; Cansell and Aymonier, 2009), the consortium [composed of ICMCB, GET and IMERYS] developed a semi-industrial pilot facility that met the group's as well as industry's expectations in demand, being able to produce sufficient quantities to perform application tests. This process takes advantage of the specific properties of water, which is neither a liquid nor a gas under supercritical conditions (above 374 °C and 221 bars). The hydrothermal reaction is indeed a precipitation reaction, as described in Fig. 4. The principle of the hydrothermal reactor (Fig. 5), which operates in continuous mode under supercritical conditions, is as follows: a precipitation reaction involving sodium metasilicate and magnesium acetate (plus acetic acid and sodium acetate) is carried out (with a ratio of 4 Si for 3 Mg in order to produce talc, for example). Then, high pressure pumps drive this precipitate to a reactor where supercritical water conditions prevail between 10 and 60 s at most (controlled by a pressure regulator). The resulting product is then either recovered directly (followed by 3 to 4 successive washes to remove

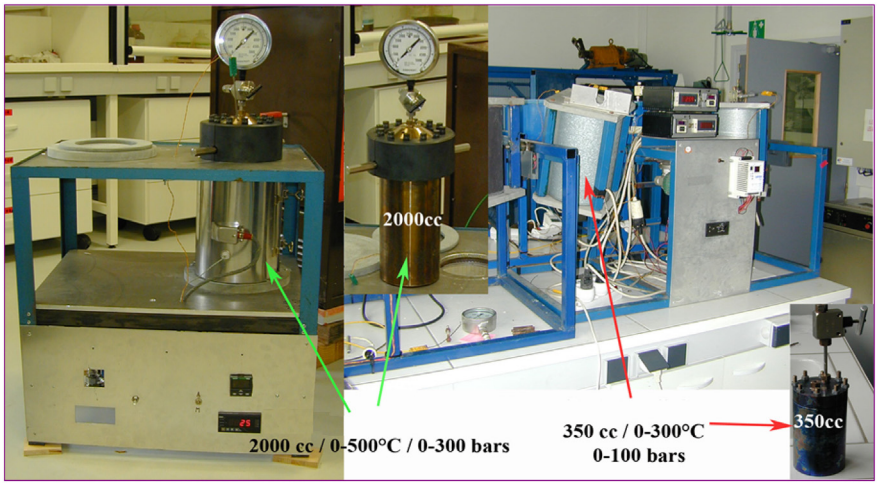

Fig. 2. Different batch type reactors from 350 to 2000 cc for temperatures ranging from 0 to 500 °C and maximum pressures of 300 bar.

Fig. 3. 18 L batch reactor implanted at GET and owned by IMERYS.

excess sodium acetate) or passed through a ceramic sinter that separates the product formed from the residual sodium acetate (Dumas et al., 2016; Claverie et al., 2018).

In our example, the product obtained is talc with a basal line located at 9.6Å (Fig. 6), higher than reference natural talc thanks to the particles size of the final product (Fig. 7) which is lower than 1 µm, with two populations centered around 90 nm and 240 nm. A transmission electron microscopy image of a synthetic talc is shown in Fig. 8. It is well defined, with a stack of layers visible in the c* direction (8 nm), with homogeneous fine particle size at around 45 nm. Scanning electron microscopy (Fig. 9) confirms the TEM observation. These electron microscopy images tell us about the morphology of the synthesized particles, in particular a strong extension in the (a, b) plane with respect to the stacking along the c* axis (less than a dozen of sheets). Thus, the products have a high aspect ratio, which is an important physical feature to consider for their insertion into composite matrices, such as polymers.

As soon as the system is in supercritical conditions, the run products are obtained after very short reaction times, typically between 10 and 60 s (Dumas et al., 2016; Claverie et al., 2018). In Fig. 10, it is easy to observe that talc is formed above the supercritical conditions of water, whereas below these conditions, a poorly crystallized phase

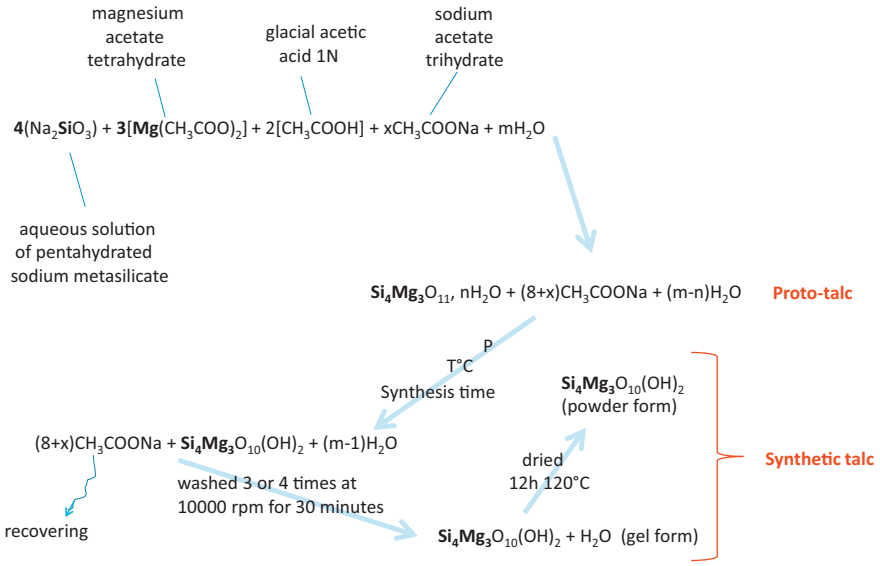

Fig. 4. Reaction of precipitation leading to the formation of proto-talc and then to the synthesis of talc.

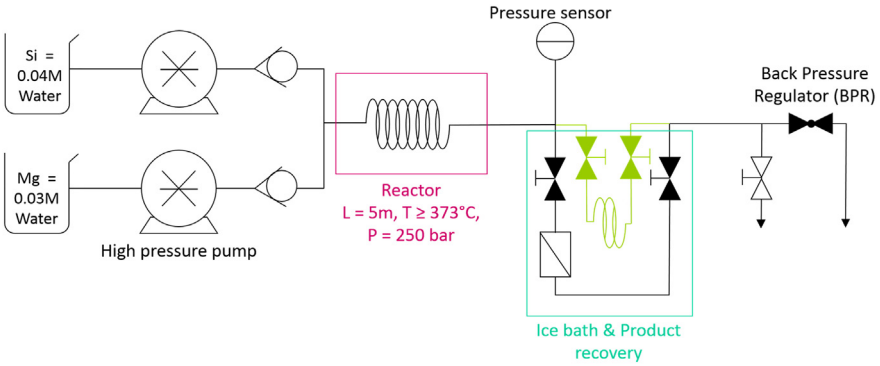

Fig. 5. Conceptual diagram of the phyllosilicate synthesis in continuous mode under supercritical conditions.

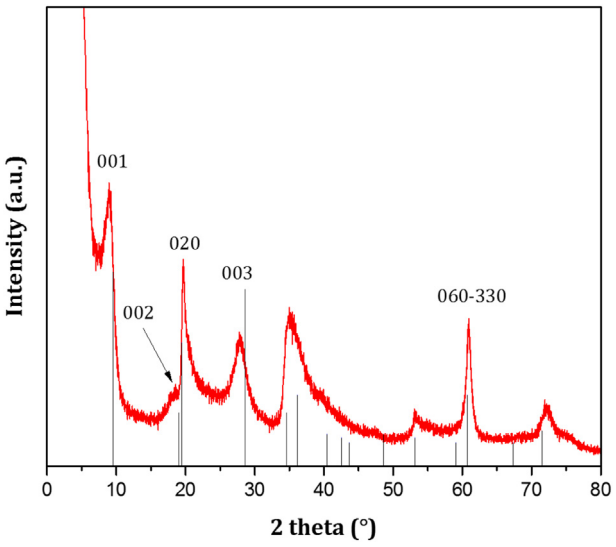

Fig. 6. X-ray diffractogram of a talc synthesized in supercritical water for a time of 20 s. Red: synthetic talc. Black: X-ray lines of natural talc. (For interpretation of the references to color in this figure legend, the reader is referred to the web version of this article.)

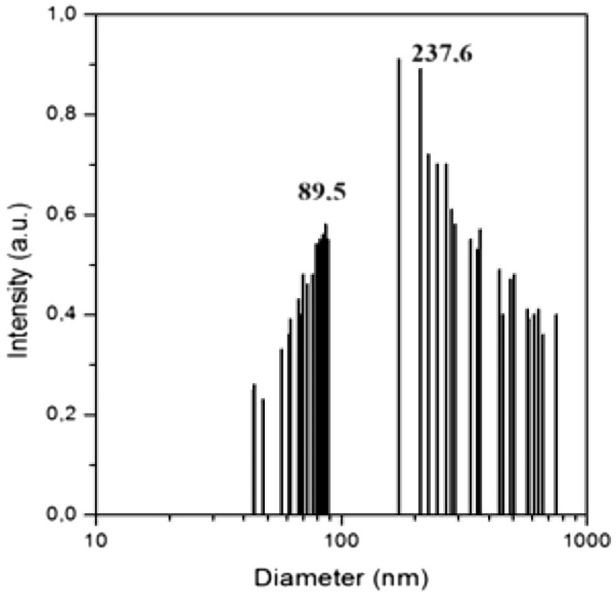

Fig. 7. Particle size distribution of a talc synthesized in supercritical water for a time of 20 s.

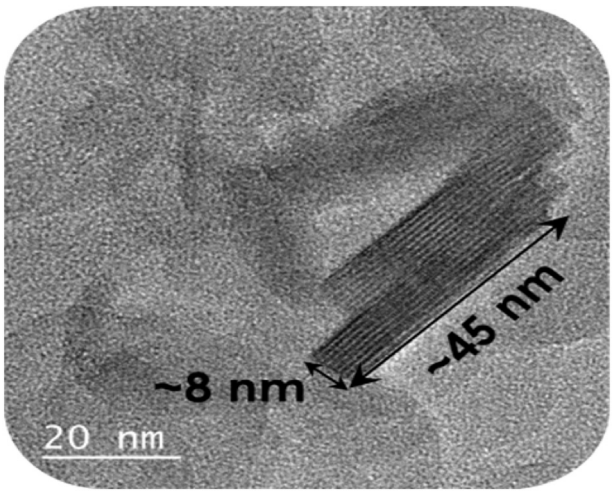

Fig. 8. Transmission electron microscopy image of a talc synthesized in supercritical water for a time of 20 s.

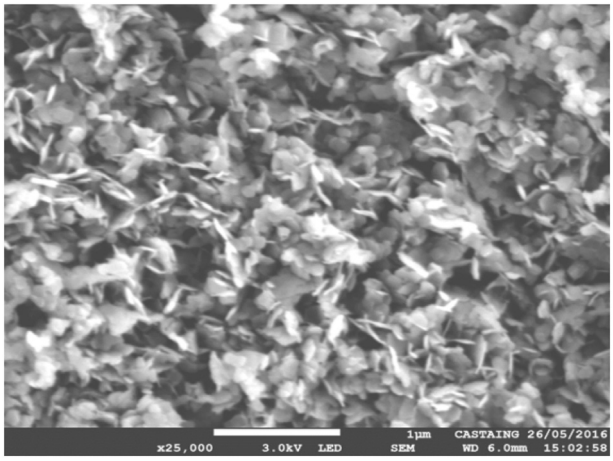

Fig. 9. Scanning electron microscope image of a talc synthesized in supercritical water for a time of 20 s.

(amorphous) called proto-talc forms. The samples synthesized under supercritical conditions (TF-38023 and TF-40023) exhibit the 001, 020–110, 003, and 060–330 reflections characteristic of the talc structure. At lower temperature (TF-35020), the 00ℓ reflections of talc are almost nonexistent and only the 020–110 and 060–330 reflections of clays are developed. The crystallinity of sample TF-40023 is comparable to that of the synthetic talc sample obtained in a batch reactor running 2 h at 300 °C and 85 bar. When the reaction time is reduced by half (TF-40010), talc of lower crystallinity is obtained. A specific

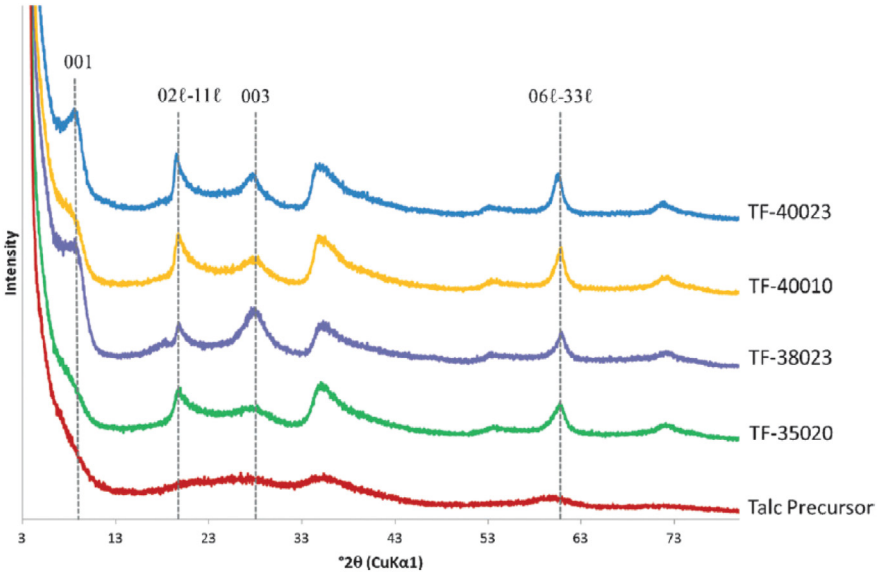

Fig. 10. XRD patterns of synthetic talc samples obtained using the supercritical hydrothermal flow synthesis process. XRD patterns of samples obtained by varying temperature (350 °C (green), 380 °C (purple), 400 °C (yellow and blue)), or synthesis time (10 s (yellow) and 20 or 23 s (green, purple, and blue)). The XRD of proto-talc (red) is named as talc precursor. From Dumas et al. (2016). (For interpretation of the references to color in this figure legend, the reader is referred to the web version of this article.)

Fig. 11. Synthetic talc powder (left) and aqueous gel of synthetic talc (right).

particularity of synthetic talcs, compared to their natural counterparts, is the perfect equilibrium of their particles in an aqueous medium, implying that the synthetic product is in the form of an aqueous or hydroalccolic gel (Fig. 11 on the right), due to the hydrophilic nature of synthetic talc. Conversely, the strongly hydrophobic natural talc precipitates under the same conditions. Drying and grinding of the synthetic talc produces a white powder (Fig. 11 on the left), which, by wetting it, can be resuspended to make a synthetic talc gel again. This reversibility is an undeniable advantage of synthetic talc over natural talc.

This property can be explained by the fact that the submicrometer-size particles of synthetic talc have much higher BET values (220 to 600 $m^2 \cdot g^{-1}$) than natural talcs ($\leq$ 20 $m^2 \cdot g^{-1}$), because of their higher exchange surface and higher ratio of hydrophilic lateral borders to hydrophobic basal surfaces. Also, the edges are the location of silanol (SiOH) and MgOH groups. Thus, the borders have significant amounts of physisorbed water (up to 14%; determined by differential thermal gravity), resulting in an equilibrium with the aqueous medium (Fig. 12) and gel formation.

3. Octahedral substitutions: From proto-talc to talc

The chemistry of the synthesis process makes it possible to replace divalent Mg atoms, in part or totally, by other divalent atoms such as Ni, Co, Cu, Fe and Mn. (Fig. 13). Whatever the octahedral cation, the obtained products are talcs, and many studies have shown occurrence of solid solutions between end-members (Ni, Mg, Fe^{2+}, …)$_3$ $Si_4O_{10}(OH)_2$ (Martin et al., 1992; Petit et al., 1995, 2004a; Corona et al., 2015). It is thus possible to obtain synthetic talc compounds that are colored to the core. Fig. 14 shows the comparison between a natural pink talc from China (François Martin's personal collection), and a green synthetic talc in which Mg was replaced by Ni. The natural sample loses its color after grinding (like the colored talc samples studied by Misch et al., 2018, this talc is very pure and contains no minerals that could explain the pink color, which is probably due to the arrangement of crystallites in the bulk ore inducing a light reflection phenomenon) while the synthetic Ni sample retains its green color.

The paper of Dumas et al. (2015b), based on the superior visibility of Ni in EXAFS spectroscopy with respect to Mg, aimed to first understand the genesis of Ni-rich talc from nucleation to crystal growth. All of the characterization methods showed that, with synthesis duration, talc progressively structured to a local (FTIR, EXAFS) or an extended (crystalline) order (XRD). Talc growth unit is constituted by 2–3 Ni-octahedra 3.07 Å apart, and 3–4 Si-tetrahedra distributed on the top and bottom of the octahedral "sheet" and distanced from Ni by 3.29 Å. This "nano-talc" entity is the result of talc precipitation. With the synthesis duration, these talc units get interlocked through the octahedral sheet. Simultaneously, the tetrahedral sheets grow, and Si—O—Si chains are progressively formed. At 300 °C in classic batch reactor, or above supercritical conditions, the synthesis time only influences the particle size at the local order. The mixing of starting material and its impact on the cationic distribution reveal that, independently of the proto-talc preparation, a random distribution between octahedral cations is obtained at 300 °C. Contrary to previous statements in the literature (Decarreau et al., 1989), no cluster formation was evidenced at low temperatures.

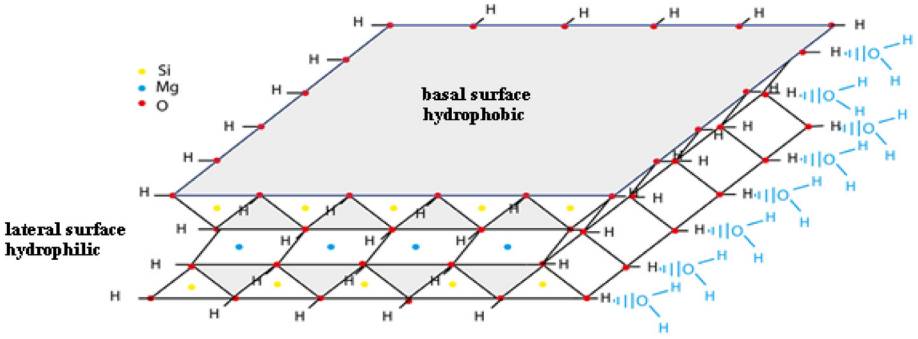

Fig. 12. Diagram of hydrophilic borders and hydrophobic surfaces of synthetic talc. The scheme has sizes of 4 nm^2 of area over 1 nm thick and is not the representation of a synthesized particle (size at least 10 times larger in the (ab) plane).

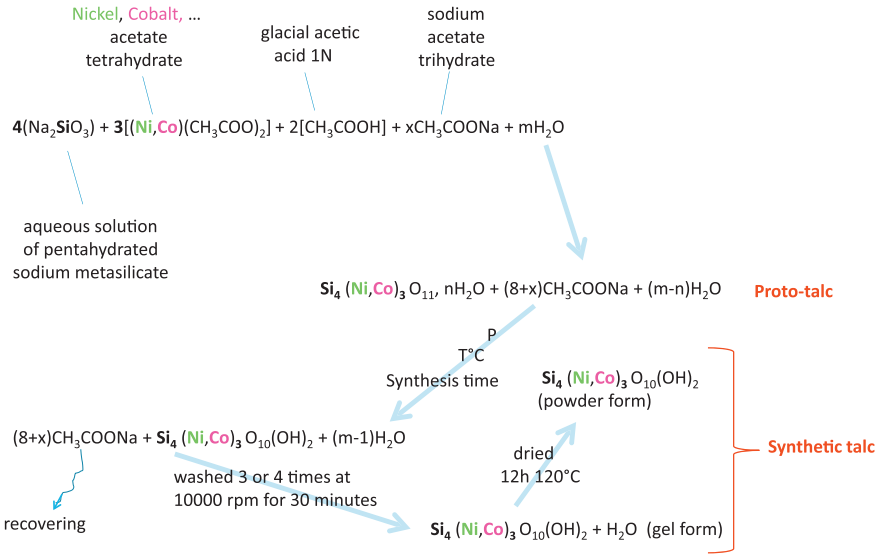

Fig. 13. Reaction precipitation leading to the formation of (Ni, Co, …)-bearing proto-talc and then to the synthesis of (Ni, Co, …)-bearing talc.

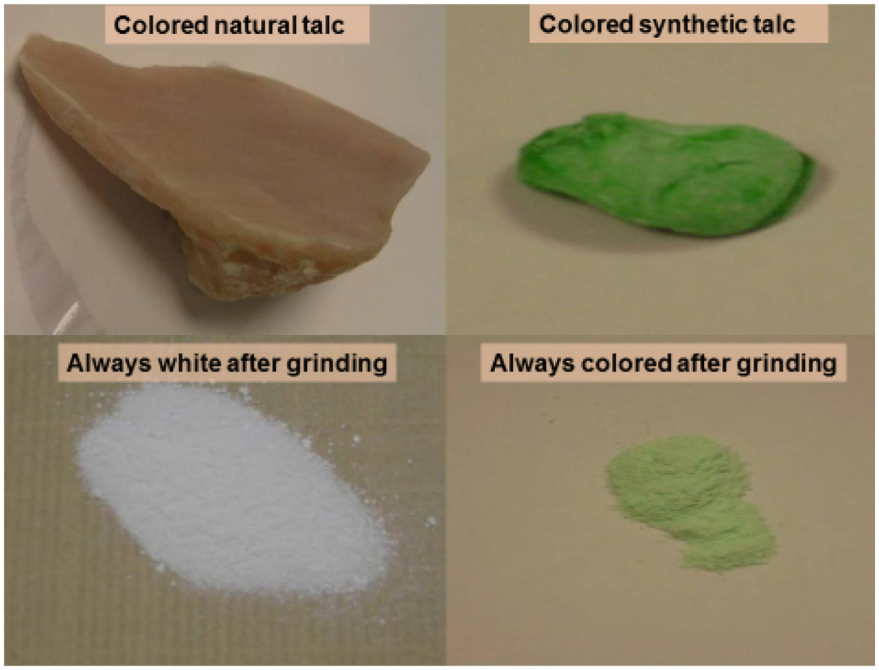

Fig. 14. Pink natural talc (left) and green synthetic talc (right) and their respective powder after grinding. (For interpretation of the references to color in this figure legend, the reader is referred to the web version of this article.)

Fig. 15. Examples of synthetic talc colors by partial or complete substitution of magnesium by others divalent cations.

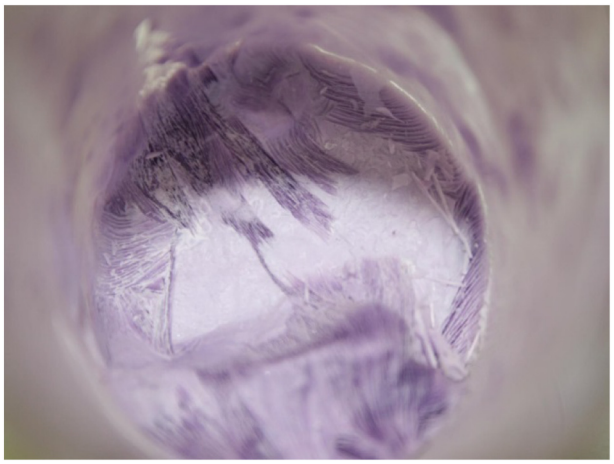

Fig. 16. Co-bearing talc with shiny appearance.

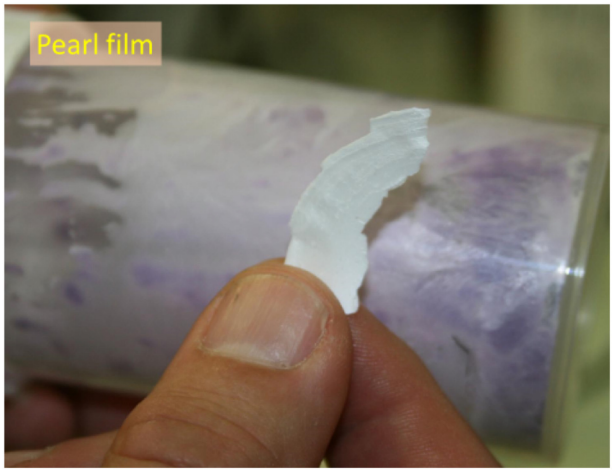

Fig. 17. Pearl film of Ni-Mg-bearing talc.

Accessing a wide range of colors is possible just by the set of substitutions (Fig. 15). Visual aspect can also be modified. For instance, synthetic Co-talcs (Fig. 16) not only present the pearled and shiny aspect of natural talcs, but they form films that keep these visual properties after pressing (Fig. 17). An interesting and unexpected aspect of this game of substitutions is that it may lead to products with new physical characteristics, such as low-temperature permanent magnetism for samples with Ni.

Remarkably, nano-divided mineral products can also be inserted in the surface of synthetic talc to endow particles with electrical conduction (Bonino et al., 2012) or magnetic properties. For example, synthetic talc particles displaying valuable magnetism at room temperature were obtained by inserting nano-magnetites on their borders by a one-pot process (Fig. 18) (Dumas et al., 2011b).

4. Dispersion in polymer matrix

In principle, the adsorption of various molecules, atoms and mineral phases can be envisaged in order to confer new chemical and physical properties to synthetic talcs. For instance, colored and/or fluorescent organic molecules have been successfully adsorbed on synthetic talc particles (Aymonier et al., 2017a, 2017b). Of course, the amount of adsorbed species can be much larger on synthetic talcs than on natural talcs, because of increased specific surface and extended borders where SiOH and MgOH groups favor hydrogen bonds and electrostatic interactions. Synthetic talcs thus present original physical behaviors and functionalities, which are highly sought after by manufacturers, in order to develop new composite materials. Polymers are materials in which these nanoparticles are of particular interest. Indeed, introducing a small and well dispersed mineral filler allows the mechanical strength and other physical or chemical parameters of polymers to be improved. Many studies done with talcs and natural clays have shown the interest of using these micrometric mineral fillers. Recently, a large number of polymer stability studies have been carried out using synthetic talc fillers, and they have shown the superiority of these submicrometric particles.

To the best of our knowledge, no Ni-rich talc particles have been introduced in polymers yet. However, the following example suggests that it may be possible to do so. Using synthetic talc or Fe_3O_4-synthetic talc as filler in the synthesis of polyurethane by physical mixture, Dias et al. (2015, 2016) and Dos Santos et al. (2015) obtained

Fig. 18. Magnetic synthetic talc attracted by the magnet. Note that all the powder is attracted to the magnet.

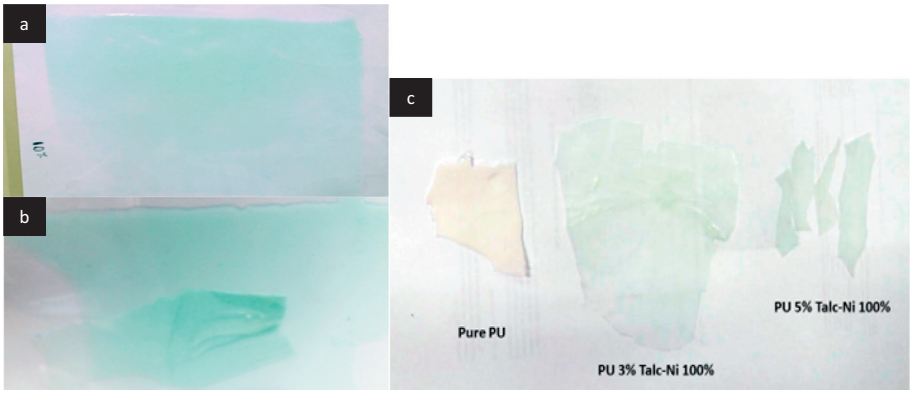

Fig. 19. Polyurethane films with various Ni-bearing talc contents: a) homogeneous distribution of nano-charges; b) heterogeneous distribution of nano-charges; c) films containing low talc charge.

nanocomposites in which the mineral filler was well dispersed into the polyurethane matrix, even at high filler content of 10 wt%. These composite materials showed superior crystallization temperature and thermal stability. Synthetic talc gel (Dias et al., 2018) and nano-Fe_3O_4-synthetic talc gel (Dos Santos et al., 2018) was also incorporated into a waterborne polyurethane (WPU) matrix, which is much more environmentally friendly than its solvent-based analogue. For example, in the case of nano-Fe_3O_4-synthetic talc gel, the obtained composite displayed a typical ferromagnetic behavior below Curie temperature (about 120 K), a superparamagnetic behavior above this temperature and superior mechanical properties compared to solvent-based nanocomposites. Synthetic talcs manufactured in nano-gel form are particularly interesting because their interaction with water favors the dispersion of the fillers within the WPU matrix.

The high surface area of synthetic talc plays a significant role in the increase of crystallinity and thermal properties of nanocomposites, provided that the nano-fillers are well dispersed or are exfoliated into the various polymer matrices, which is generally the case (Yousfi et al., 2013, 2014, 2015). However, the dispersion of nanometric charges is often difficult to measure without using expensive investigations techniques (SEM, TEM, AFM, …). Magnesium synthetic talc are white, just like the polymer matrices, and the submicrometer size makes the particles very difficult to observe by optical methods. A simple solution is to replace Mg with Ni or with another divalent element, to obtain a colored powder or gel (Prado et al., 2015). Fig. 19a shows a sample of polyurethane loaded with 10% Ni talc. The homogeneous green color suggests that the nano-charges are well dispersed. On the other hand, for the same concentration, in Fig. 19b, a segregation of the nano-charges has taken place during the preparation of the polyurethane film, and the coloration is irregular. For low nano-charge concentrations, the good dispersions of nano-charges in the matrix can be observed with the naked eye (Fig. 19c).

5. Mineral synthesis: hints to the understanding the Ni- and Co-rich lateritic environments

From the above sections, the interest of incorporating Ni, Co, or other divalent elements into talc, is obvious. Another potential of this practice is that synthetic crystal growth is a proxy to natural processes. In natural environments, Ni-rich mineral phases constitute the so-called garnierite Ni-ores. In most of the New Caledonia occurrences, these are dominated by talc-like minerals, also called kerolite or pimelite depending on the relative concentration of Mg and Ni. The Ni—Mg kerolite solid solution varies between the two end-members, e.g. Mg-rich kerolite to Ni-rich pimelite (Cathelineau et al., 2015, 2016, 2017; Myagkiy et al., 2017; Quesnel et al., 2017). Kerolite has a structure close to that of talc, with an interlayer distance of ~9.5 Å, but it is characterized by an excess of Mg in the octahedral site and a relative deficit of Si in the tetrahedral site (Brindley et al., 1979). Its H_2O content is also higher than that in talc and an ideal chemical formula is: $(Ni,Mg)_{3+x}(Si_{4-y})O_{10}(OH)_2{\cdot}nH_2O$, where x = 2y and n ~ 1.

The solid solution between the Ni and Mg end-members is complete, corresponding to a Ni—Mg substitution in the octahedral sheet. Raman spectra in the OH stretching vibration region have been recorded on representative samples from Ni-ores in New-Caledonia, covering the whole range of Ni—Mg substitution (Cathelineau et al., 2015). This study shows a continuous and significant evolution from the Mg to the Ni end-member and reveals that four possible arrangements of Ni and Mg in the octahedral sheet are encountered, these arrangements being dependent on the Ni—Mg substitution rate. For synthetic talcs, the formula is identical but without the water molecules, the solid solutions are also complete (Martin et al., 1992, 1996; Martin, 1994; Petit et al.,

2004a, 2004b; Dumas, 2013; Dumas et al., 2015b). The difference between talc and kerolites is very small, and the question is whether natural kerolites are more like synthetic talcs or synthetic proto-talcs. Substitutions, complete and continuous solid solutions between the Mg and Ni poles are arguments to say that the phenomena of the natural environment are similar to those of hydrothermal laboratory processes. In both natural and synthetic cases, a random distribution was observed but no cluster distribution.

The similarities between crystal growth in natural environments and in a synthetic medium will prompt us to compare the three major phases, namely proto-talc, synthetic talc and natural kerolites, in the course of further work. The results will be essential to clarify the synthesis processes during the transition to industrial production. Indeed, mineral fillers are vastly used because they allow the material's properties to be much improved, in addition to lowering the price of the material in which they are inserted. If the size of the conventional inorganic fillers is micrometric or multi-micrometric, the tests with nano-divided charges show an increase of certain properties if and only if these charges are uniformly distributed in the composite materials. The work on the new fillers will open the possibility of moving the dozen patents on hydrophilic sub-micron charges filed by L'OREAL into production. Incorporation of these charges can modify the rheology of certain preparations, which could not be achieved using those charged with hydrophobic natural minerals.

Acknowledgements

The authors wish to acknowledge the financial support from IMERYS Company for the PhD. grants of Marie Claverie and Mathilde Poirier and CAPES (Brazil government) for PhD scholarship of Manoela Argenton Prado, and Guilherme Dias and CNPq for DT grant (number 303467/2015-0).

References

Arseguel, D., Bonino, J.-P., Decarreau, A., Ferrage, E., Ferret, J., Grauby, O., Lebre, C., Martin, F., Petit, S. (2006) Method for preparing talcose compositions comprising synthetic mineral particles containing silicon, germanium and metal. Patents FR2903680, WO2008009799.

Aymonier, C., Erriguible, A., Marre, S., Serani, A., Cansell, F., 2007. Processes using supercritical fluids: a sustainable approach for the design of functional nanomaterials. Int. J. Chem. React. Eng. 5, A77.

Aymonier, C., Dumas, A., Le Roux, C., Martin, F., Micoud, P., Poirier M., Slostowski, C. (2014) Process for the continuous preparation of phyllomineral synthetic particles. Patents FR3019813, WO2015159006.

Aymonier, C., Fery-Forgues, S., Le Roux, C., Martin, F., Micoud, P., Poirier M. (2017a) Coloured organic/inorganic hybrid materials and method for preparing same. Patents FR3062074, WO2018138148.

Aymonier, C., Fery-Forgues, S., Le Roux, C., Martin, F., Micoud, P., Poirier M. (2017b) Photoluminescent hybrid organic/inorganic materials and method for preparing same. Patent FR3062073, WO2018138153.

Baba, A.A., Ibrahim, A.S., Bale, R.B., Adekola, F.A., Alabio, A.G.F., 2015. Purification of a Nigerian talc ore by acid leaching. Appl. Clay Sci. 114, 476–483. https://doi.org/10.1016/j.clay.2015.06.031.

Bacchin, P., Bonino, J.P., Martin, F., Combacau, M., Barthes, P., Petit, S., Ferret, J., 2006. Surface pre-coating of talc particles by carboxyl methyl cellulose adsorption: Study of adsorption and consequences on surface properties and settling rate. Colloids Surf. A Physicochem. Eng. Asp. 272, 211–219. https://doi.org/10.1016/j.colsurfa.2005.07.026.

Bonino, J. P., Bacchin, P., Martin, F., Barthes, P., Ferrage, E., Vautrin, W., Vaillant, S. (2002) Composite material consisting of a metal matrix and talc. Patent FR2848219, WO2004063428.

Bonino, J.P., Dumas, A., Flahaut, E., Fraichard, L., Greenhill-Hooper, M., Gressier, M., Martin, F. and Menu, M.J. (2012) Talc composition. Patent EP2747091, WO2014096203.

Borges, R., Dutra, L.M., Barison, A., Wypych, F., 2016. MAS NMR and EPR study of structural changes in talc and montmorillonite induced by grinding. Clay Miner. 51, 69–80. https://doi.org/10.1180/claymin.2016.051.1.06.

Brindley, G.W., Bish, D.L., Wan, H.M., 1979. Compositions, structures, and properties of nickel-containing minerals in the kerolite-pimelite series. Am. Mineral. 64, 615–625.

Cansell, F., Aymonier, C., 2009. Design of functional nanostructured materials using supercritical fluids. J. Supercrit. Fluids 47, 508–516. https://doi.org/10.1016/j.supflu.2008.10.002.

Castillo, L.A., Barbosa, S.E., Maiza, P., Capiati, N.J., 2014. Integrated process for Purification of Low Grade Talc Ores. 32. pp. 1–7. https://doi.org/10.1080/02726351.2012.755588.

Cathelineau, M., Caumon, M.C., Massei, F., Brie, D., Harlaux, M., 2015. Raman spectra of Ni-Mg kerolite: effect of Ni-Mg substitution on O-H stretching vibrations. J. Raman Spectrosc. 46 (10), 933–940. https://doi.org/10.1002/jrs.4746.

Cathelineau, M., Quesnel, B., Gautier, P., Boulvais, P., Couteau, C., Drouillet, M., 2016. Nickel dispersion and enrichment at the bottom of the regolith: formation of pimelite target-like ores in rock block joints (Koniambo Ni deposit, New Caledonia). Mineral. Deposita 51 (2), 271–282. https://doi.org/10.1007/s00126-015-0607-y.

Cathelineau, M., Myagkiy, A., Quesnel, B., Boiron, M.C., Gautier, P., Boulvais, P., Ulrich, M., Truche, L., Golfier, F., Drouillet, M., 2017. Multistage crack seal vein and hydrothermal Ni enrichment in serpentinized ultramafic rocks (Koniambo massif, New Caledonia). Mineral. Deposita 52 (7), 945–960. https://doi.org/10.1007/s00126-016-0695-3.

Cavajda, V., Uhlik, P., Derkowski, A., Caplovicova, M., Madejova, J., Mikula, M., Ifka, T., 2015. Influence of grinding and sonication on the crystal structure of talc. Clay Clay Miner. 63 (4), 311–327. https://doi.org/10.1346/CCMN.2015.0630405.

Chabrol, K., Gressier, M., Pebere, N., Menu, M.J., Martin, F., Bonino, J.P., Marichal, C., Brendle, J., 2010. Functionalization of synthetic talc-like phyllosilicates by alkoxyorganosilane grafting. J. Mater. Chem. 20, 9695–9706. https://doi.org/10.1039/c0jm01276a.

Claverie, M., Dumas, A., Carême, C., Poirier, M., Le Roux, C., Micoud, P., Martin, F., Aymonier, C., 2018. Synthetic talc and talc-like structures: preparation, features and applications. Chem. Eur. J. 24, 519–542. https://doi.org/10.1002/chem.201702763.

Corona, J.C., Jenkins, D.M., Dyar, M.D., 2015. The experimental incorporation of Fe into talc: a study using X-ray diffraction, Fourier transform infrared spectroscopy, and Mössbauer spectroscopy. Contrib. Mineral. Petrol. 170, 29. https://doi.org/10.1007/s00410-015-1180-1.

Decarreau, A., Mondesir, H., Besson, G., 1989. Synthesis and stability of Mg and Ni stevensite, kerolite and talcs between 80°C and 240°C. C. R. Acad. Sci., Ser. III 308, 301–306.

Dellisanti, F., Valdre, G., Mondonico, M., 2009. Changes of the main physical and technological properties of talc due to mechanical strain. Appl. Clay Sci. 42, 398–404. https://doi.org/10.1016/j.clay.2008.04.002.

Dias, G., Prado, M.A., Carone, C., Ligabue, R., Dumas, A., Martin, F., Le Roux, C., Micoud, P., Einloft, S., 2015. Synthetic silico-metallic mineral particles (SSMMP) as nanofillers: comparing the effect of different hydrothermal treatments on the PU/SSMMP nanocomposites properties. Polym. Bull. 72 (11), 2991–3006. https://doi.org/10.1007/s00289-015-1449-6.

Dias, G., Prado, M., Carone, C., Ligabue, R., Dumas, A., Le Roux, C., Micoud, P., Martin, F., Einloft, S., 2016. Comparing different synthetic talc as fillers for polyurethane nanocomposites. Macromol. Symp. 367, 136–142. https://doi.org/10.1002/masy.201500141.

Dias, G., Prado, M., Le Roux, C., Poirier, M., Micoud, P., Ligabue, R., Martin, F., Einloft, S., 2018. Analyzing the influence of different synthetic talcs in waterborne polyurethane nanocomposites obtainment. J. Appl. Polym. Sci. 135 (14), 46107. https://doi.org/10.1002/app.46107.

Dietemann, M., 2012. Etude de la précipitation du silicate de magnésium amorphe assistée par ultrasons: synthèse, caractérisation et modélisation. PhD thesis. University of Toulouse - INP, France.

Dietemann, M., Baillon, F., Espitalier, F., Calvet, R., Accart, P., Del Confetto, S., Greenhill-Hooper, M., 2013. Evaluation of the physico-chemical properties of an amorphous magnesium silicate synthesized by an ultrasound-assisted precipitation. Chem. Eng. J. 215–216, 658–670. https://doi.org/10.1016/j.cej.2012.11.079.

Dos Santos, L.M., Ligabue, R., Dumas, A., Le Roux, C., Micoud, P., Meunier, J.F., Martin, F., Einloft, S., 2015. New magnetic nanocomposites: polyurethane/Fe_3O_4-synthetic talc. Eur. Polym. J. 69, 38–49. https://doi.org/10.1016/j.eurpolymj.2015.05.026.

Dos Santos, L.M., Ligabue, R., Dumas, A., Le Roux, C., Micoud, P., Meunier, J.F., Martin, F., Corvo, M., Almeida, P., Einloft, S., 2018. Waterborne polyurethane/Fe_3O_4-synthetic talc composites: synthesis, characterization, and magnetic properties. Polym. Bull. 75, 1915–1930. https://doi.org/10.1007/s00289-017-2133-9.

Dublet, G., Juillot, F., Brest, J., Noël, V., Fritsch, E., Proux, O., Olivi, L., Ploquin, F., Morin, G., 2017. Vertical changes of the Co and Mn speciation along a lateritic regolith developed on peridotites (New Caledonia). Geochim. Cosmochim. Acta 217, 1–15. https://doi.org/10.1016/j.gca.2017.07.010.

Dumas, A., 2013. Elaboration de nouveaux procédés de synthèse et caractérisation de talcs sub-microniques: de la recherche fondamentale vers des applications industrielles. PhD Thesis. University of Toulouse III - Paul Sabatier, France.

Dumas, A., Le Roux, C., Martin, F., Micoud, P. (2011a) Process for preparing a composition comprising synthetic mineral particles and composition. Patents FR2977580, WO2013004979.

Dumas, A., Gardes, E., Le Roux, C., Martin, F., Micoud, P. (2011b) Process for preparing a magnetic talcous composition and magnetic talcous composition. Patents FR2984872, WO2013093376.

Dumas, A., Martin, F., Ferrage, E., Micoud, P., Le Roux, C., Petit, S., 2013a. Synthetic talc advances: coming closer to nature, added value and industrial requirements. Appl. Clay Sci. 85, 8–18. https://doi.org/10.1016/j.clay.2013.09.006.

Dumas, A., Martin, F., Le Roux, C., Micoud, P., Petit, S., Ferrage, E., Brendle, J., Grauby, O., Greenhill-Hooper, M., 2013b. Phyllosilicates synthesis: a way of accessing edges contributions in NMR and FTIR spectroscopies. Example of synthetic talc. Phys. Chem. Miner. 40, 361–373. https://doi.org/10.1007/s00269-013-0577-5.

Dumas, A., Martin, F., Ngo Ke, T., Nguyen Van, H., Nguyen Viet, D., Nguyen Tat, V., Kieu Quy, N., Micoud, P., de Parseval, P., 2015a. The crystal-chemistry of Vietnamese talcs from the Thanh Son district (Phu Tho province, Vietnam). Clay Miner. 50, 607–617. https://doi.org/10.1180/claymin.2015.050.5.05.

Dumas, A., Mizrahi, M., Martin, F., Requejo, F.G., 2015b. Local and extended-order evolution of synthetic talc during hydrothermal synthesis: extended X-ray absorption

fine structure, X-ray diffraction, and Fourier transform infrared spectroscopy studies. Cryst. Growth Des. 15, 5451–5463. https://doi.org/10.1021/acs.cgd.5b01076.
Dumas, A., Claverie, M., Slostowski, C., Aubert, G., Careme, C., Le Roux, C., Micoud, P., Martin, F., Aymonier, C., 2016. Fast-geomimicking using chemistry in supercritical water. Angew. Chem. Int. Ed. 55, 9868–9871. https://doi.org/10.1002/anie.201604096.
Godet, L., 2001. Broyage fin du talc par jets d'air opposés. PhD thesis. University of Lorraine - INPL, France.
Kloprogge, J.T., Komarneni, S., Amonette, J.E., 1999. Synthesis of smectite clay minerals: a critical review. Clay Clay Miner. 47, 529–554. https://doi.org/10.1346/CCMN.1999.0470501.
Kojima, Y., Usuki, A., Kawasumi, M., Okada, A., Fukushima, Y., Kurauchi, T., Kamigaito, O., 1993a. Mechanical properties of Nylon-6 clay hybrid. J. Mater. Res. 8, 1185–1189. https://doi.org/10.1557/JMR.1993.1185.
Kojima, Y., Usuki, A., Kawasumi, M., Okada, A., Kurauchi, T., Kamigaito, O., 1993b. Sorption of water in Nylon-6 clay hybrid. J. Appl. Polym. Sci. 49, 1259–1264. https://doi.org/10.1002/app.1993.070490715.
Le Roux, C., Martin, F., Micoud, P., Dumas, A. (2010) Method for preparing a composition including synthetic inorganic particles. Patents FR2969594, WO2012085239.
Lèbre, C., 2007. Elaboration et caractérisation de talcs synthétiques pour l'amélioration des propriétés physiques des matériaux composites industriels. PhD Thesis. University of Toulouse III - Paul Sabatier, France.
Liao, J., Senna, M., 1992. Thermal behavior of mechanically amorphized talc. Thermochim. Acta 197, 295–306.
Martin, F., 1994. Etude cristallographique et cristallochimique de l'incorporation du Germanium et du Gallium dans les phyllosilicates: approche par synthèse minérale. PhD thesis. University of Aix-Marseille, France.
Martin, F., Petit, S., Grauby, O., Noack, Y., Hazemann, J.L., Decarreau, A., 1992. Experimental study of Si-Ge tetrahedral solid solution in Ni-Co-Mg talcs. Thin Solid Films 222, 189–195.
Martin, F., Ildefonse, P., Hazemann, J.L., Petit, S., Grauby, O., Decarreau, A., 1996. Random distribution of Ge and Si in synthetic talc: an EXAFS and FTIR study. Eur. J. Mineral. 8, 289–299.
Martin, F., Ferret, J., Lèbre, C., Petit, S., Grauby, O., Bonino, J.P., Arseguel, D., Decarreau, A., Ferrage, E. (2006) Method for preparing a synthetic talc composition from a kerolite composition. Patents FR2903682, WO2008009801.
Misch, D., Pluch, H., Mali, H., Ebner, F., Hui, H., 2018. Genesis of giant Early Proterozoic magnesite and related talc deposits in the Mafeng area, Liaoning Province, NE China. J. Asian Earth Sci. 160, 1–12. https://doi.org/10.1016/j.jseaes.2018.04.005.
Myagkiy, A., Truche, L., Cathelineau, M., Golfier, F., 2017. Revealing the conditions of Ni mineralization in the laterite profiles of New Caledonia: insights from reactive geochemical transport modelling. Chem. Geol. 466, 274–284. https://doi.org/10.1016/j.chemgeo.2017.06.018.
Petit, S., Robert, J.L., Decarreau, A., Besson, G., Grauby, O., Martin, F., 1995. Contribution of spectroscopic methods to 2:1 clay characterization. Bull. Centres Rech. Explor. Prod. Elf-Aquitaine 19 (1), 119–148.
Petit, S., Decarreau, A., Martin, F., Buchet, R., 2004a. Refined relationship between the position of the fundamental OH stretching and the first overtones for clays. Phys. Chem. Miner. 31, 585–592. https://doi.org/10.1007/s00269-004-0423-x.
Petit, S., Martin, F., Wiewiora, A., de Parseval, P., Decarreau, A., 2004b. Crystal-chemistry of talc: a near infrared (NIR) spectroscopy study. Am. Mineral. 89, 319–326. https://doi.org/10.2138/am-2004-2-310.
Prado, M.A., Dias, G., Carone, C., Ligabue, R., Dumas, A., Le Roux, C., Micoud, P., Martin, F., Einloft, S., 2015. Synthetic Ni-talc as filler for producing polyurethane nanocomposites. J. Appl. Polym. Sci. 132 (16), 41854. https://doi.org/10.1002/app.41854.
Quesnel, B., Le Carlier de Veslud, C., Boulvais, P., Gautier, P., Cathelineau, M., Drouillet, M., 2017. 3D modeling of the laterites on top of the Koniambo Massif, New Caledonia: refinement of the per descensum lateritic model for nickel mineralization. Mineral. Deposita 52 (7), 961–978. https://doi.org/10.1007/s00126-017-0712-1.
Reveron, H., Elissalde, C., Aymonier, C., Bousquet, C., Maglione, M., Cansell, F., 2006. Continuous supercritical synthesis and dielectric behaviour of the whole BST solid solution. Nanotechnology 17, 3527–3532. https://doi.org/10.1088/0957-4484/17/14/028.
Robert, J.F., Fragnier, P., 1996. Talc production: an overview. Macromol. Symp. 108, 13–18. https://doi.org/10.1002/masy.19961080104.
Sanchez-Soto, P.J., Wiewiora, A., Aviles, M.A., Justo, A., Perez-Maqueda, L.A., Perez-Rodriguez, J.L., Bylina, P., 1997. Talc from Puebla de Lillo, Spain. II. Effect of dry grinding on particle size and shape. Appl. Clay Sci. 12 (4), 297–312. https://doi.org/10.1016/S0169-1317(97)00013-6.
Soriano, M., Melgosa, M., Sanchez-Maranon, M., Delgado, G., Gamiz, E., Delgado, R., 1998. Whiteness of talcum powders as a quality index for pharmaceutical uses. Color. Res. Appl. 23 (3), 178–185.
Soriano, M., Sanchez-Maranon, M., Melgosa, M., Gamiz, E., Delgado, R., 2002. Influence of chemical and mineralogical composition on color for commercial talcs. Color. Res. Appl. 27 (6), 430–440. https://doi.org/10.1002/col.10096.
Usuki, A., Kawasumi, M., Kojima, Y., Okada, A., Kurauchi, T., Kamigaito, O., 1993a. Swelling behavior of montmorillonite cation exchanged for omega-amino acids by epsilon-caprolactam. J. Mater. Res. 8 (5), 1174–1178. https://doi.org/10.1557/JMR.1993.1174.
Usuki, A., Kojima, Y., Kawasumi, M., Okada, A., Fukushima, Y., Kurauchi, T., Kamigaito, O., 1993b. Synthesis of nylon-6 clay hybrid. J. Mater. Res. 8 (5), 1179–1184. https://doi.org/10.1557/JMR.1993.1179.
Yousfi, M., Livi, S., Dumas, A., Le Roux, C., Crépin-Leblond, J., Greenhill-Hooper, M., Duchet-Rumeau, J., 2013. Use of new synthetic talc as reinforcing nanofillers for polypropylene and polyamide 6 systems: thermal and mechanical properties. J. Colloid Interface Sci. 403, 29–42. https://doi.org/10.1016/j.jcis.2013.04.019.
Yousfi, M., Livi, S., Dumas, A., Crépin-Leblond, J., Greenhill-Hooper, M., Duchet-Rumeau, J., 2014. Compatibilization of polypropylene/polyamide 6 blends using new synthetic nanosized talc fillers: morphology, thermal, and mechanical properties. J. Appl. Polym. Sci. 131 (13), 40453. https://doi.org/10.1002/app.40453.
Yousfi, M., Livi, S., Dumas, A., Crépin-Leblond, J., Greenhill-Hooper, M., Duchet-Rumeau, J., 2015. Ionic compatibilization of polypropylene/polyamide 6 blends using an ionic liquids/nanotalc filler combination: morphology, thermal and mechanical properties. RSC Adv. 5 (57), 46197–46205. https://doi.org/10.1039/c5ra00816f.
Zazenski, R., Ashton, W.H., Briggs, D., Chudkowski, M., Kelse, J.W., MacEachern, L., McCarthy, E.F., Nordhauser, M.A., Roddy, M.T., Teetsel, N.M., Wells, A.B., Gettings, S.D., 1995. Talc – occurrence, characterization, and consumer applications. Regul. Toxicol. Pharmacol. 21 (2), 218–229. https://doi.org/10.1006/rtph.1995.1032.